Continuum approach for long-wavelength acoustic phonons in quasi-two-dimensional structures

Dan Liu,[1] Arthur G. Every,[2] and David Tománek[1,*]

[1]*Department of Physics and Astronomy, Michigan State University, East Lansing, Michigan 48824, USA*

[2]*School of Physics, University of the Witwatersrand, Private Bag 3, 2050 Johannesburg, South Africa*

(Received 11 May 2016; revised manuscript received 20 September 2016; published 24 October 2016)

As an alternative to atomistic calculations of long-wavelength acoustic modes of atomically thin layers, which are known to converge very slowly, we propose a quantitatively predictive and physically intuitive approach based on continuum elasticity theory. We describe a layer, independent of its thickness, by a membrane and characterize its elastic behavior by a (3×3) elastic matrix as well as the flexural rigidity. We present simple quantitative expressions for frequencies of long-wavelength acoustic modes, which we determine using two-dimensional elastic constants calculated by *ab initio* density functional theory. The calculated spectra accurately reproduce observed and calculated long-wavelength phonon spectra of graphene and phosphorene, the monolayer of black phosphorus. Our approach also correctly describes the observed dependence of the radial breathing mode frequency on the diameters of carbon fullerenes and nanotubes.

DOI: 10.1103/PhysRevB.94.165432

I. INTRODUCTION

With the emergence of graphene as one of the hottest research topics in recent years, interest in quasi-two-dimensional (quasi-2D) materials has been rising steadily. An important characteristic of these systems is phonon spectra. State-of-the-art atomistic calculations of phonon frequencies based on *ab initio* density functional theory (DFT) start with the calculation of the Hessian (or force-constant) matrix using energy differences associated with finite displacements of all atoms in the unit cell. The phonon frequencies are then obtained from the eigenvalues of the dynamical matrix constructed from the Hessian matrix. This approach works very well for all phonons except for long-wavelength acoustic modes in quasi-2D systems. There, all practical implementations require the use of very large supercells, dense k meshes, and a highly converged basis to obtain a sufficiently accurate dynamical matrix. Even small inaccuracies caused by computer resource limitations commonly lead to imaginary frequencies in long-wavelength flexural acoustic (ZA) modes [1,2]. This artifact has nothing to do with a structural instability but is rather intrinsic to the way the dynamical matrix is constructed and diagonalized. Even though this shortcoming does not affect other modes much, its unphysical consequences have been discussed widely. So far, no practicable, predictive, and accurate alternative approach has been proposed to determine the frequency of long-wavelength ZA modes, which—among others—play an important role in the thermal conductivity of graphene nanoribbons [3].

To address the long-standing problem with the computation of long-wavelength flexural ZA modes in atomically thin layers, we propose a quantitatively predictive and physically intuitive approach based on continuum elasticity theory. We describe a layer, independent of its thickness, by a membrane and characterize its elastic behavior by a (3×3) elastic matrix as well as the flexural rigidity D. We present simple quantitative expressions for frequencies of long-wavelength acoustic ZA and—for the sake of completeness—for the longitudinal acoustic (LA) and transverse acoustic (TA) modes, which we determine using 2D elastic constants calculated by *ab initio* density functional theory. The calculated spectra accurately reproduce observed and calculated long-wavelength phonon spectra of graphene and phosphorene, the monolayer of black phosphorus. Our approach also correctly describes the observed dependence of the radial breathing mode frequency (RBM) on the diameters of carbon fullerenes and nanotubes.

The use of continuum elasticity theory as a means to determine the frequencies of long-wavelength acoustic phonons is well established [4], including its extension to plates of finite thicknesses [5,6]. Elastic constants have also been related to specific phonon modes in graphene [7–10]. Yet, independent of thickness, any plate can be mapped onto a 2D elastic membrane. Even though quantifying its elastic response to uniform static stress is all that is needed to correctly reproduce all three acoustic branches in the long-wavelength limit, this knowledge has been used only in a limited fashion to calculate phonon spectra of quasi-2D systems. In the following, we introduce a (3×3) elastic stiffness matrix for 2D membranes and relate it to the commonly used (6×6) elastic matrix for three-dimensional (3D) systems. We then derive quantitatively predictive and simple expressions for long-wavelength acoustic phonon frequencies in these structures based on the 2D elastic constants and flexural rigidity D, which we determine using static DFT calculations for the deformation energy of unit cells with few atoms. The quadratic frequency dependence on the crystal momentum for ZA and the linear dependence for LA and TA modes is quantitatively reproduced near the Brillouin-zone center using these 2D elastic constants and D. Clearly, our approach is limited to long-wavelength acoustic modes. To obtain the full phonon spectrum, these results can be combined with those of atomistic DFT calculations, which do not display convergence problems for optical and short-wavelength acoustic modes.

II. CONTINUUM APPROACH FOR LONG-WAVELENGTH ACOUSTIC MODES OF AN ELASTIC MEMBRANE

A free-standing thin slab of any substance, independent of its effective thickness, can be mapped onto an elastic

*tomanek@pa.msu.edu

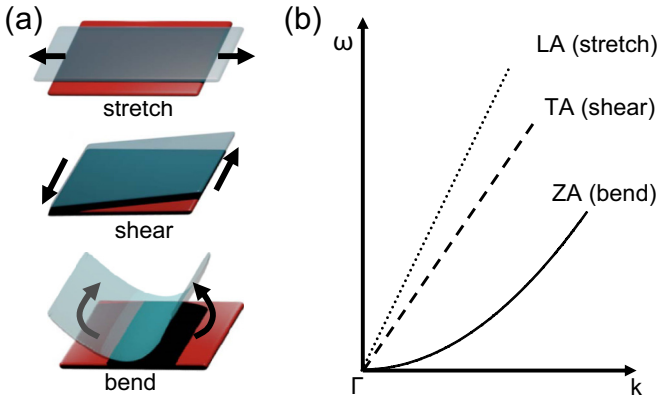

FIG. 1. (a) Schematic of possible distortions of an elastic membrane. (b) Schematic dependence of the LA, in-plane TA, and the ZA mode vibration frequencies on the crystal momentum near the center of the Brillouin zone.

membrane that resists deformations as illustrated in Fig. 1(a). In the harmonic limit, the elastic response of this two-dimensional system, considered to lie on the x-y plane, is described by the (3×3) 2D elastic stiffness matrix, which is given in Voigt notation by

$$\begin{pmatrix} c_{11} & c_{12} & 0 \\ c_{12} & c_{22} & 0 \\ 0 & 0 & c_{66} \end{pmatrix}. \tag{1}$$

c_{11} and c_{22} describe the longitudinal strain-stress relationship along the x and y directions, respectively. c_{66} describes the elastic response to in-plane shear. In an elastic isotropic plate, $c_{11} = c_{22}$, $c_{66} = (c_{11} - c_{12})/2$, and the Poisson ratio $\alpha = c_{12}/c_{11}$. In a 2D plate represented by a membrane, the dimension of the elastic stiffness constants c_{ij} is (N/m). The elastic response of the corresponding 3D system consisting of weakly interacting layers separated by interlayer spacing d_{il} is described in Voigt notation by a (6×6) C_{ij} matrix of elastic stiffness constants with the dimension (N/m^2). The relation between the two elastic matrices is given by $c_{ij} = d_{il}C_{ij}$.

The flexural response to out-of-plane stress is described by the flexural rigidity D of the plate, which may be anisotropic. D can be calculated by considering the energy cost associated with rolling up a rectangle of length L to a tube with diameter d. Assuming that L and d are large enough to ignore edge effects, we obtain

$$D = \tfrac{1}{2}\epsilon_b d^2, \tag{2}$$

where ϵ_b is the bending strain energy divided by the surface area of the tube, which is close to the area of the initial rectangle.

III. CALCULATION OF ACOUSTIC PHONON MODES OF AN ELASTIC MEMBRANE IN THE CONTINUUM LIMIT

It is well established that near the Brillouin-zone center, the frequency of LA and TA modes show a linear dependence on the crystal momentum k, whereas the ZA mode frequency increases as k^2 as seen in Fig. 1(b). As shown in the Appendix, the frequencies of the three acoustic modes of an elastic membrane can be determined quantitatively using only the elastic constants c_{11}, c_{22}, c_{66}, and D. These elastic constants can be either calculated or obtained experimentally. Also needed is the 2D mass density ρ_{2D}, which is easily determined using the atomic mass numbers and the area of the optimized unit cell.

For acoustic modes with linear dispersion, we get

$$\omega_{LA,1} = \sqrt{\frac{c_{11}}{\rho_{2D}}}k \tag{3}$$

for the LA mode along the x direction with the value of the square root giving the longitudinal speed of sound in the x direction. Similarly, we get

$$\omega_{LA,2} = \sqrt{\frac{c_{22}}{\rho_{2D}}}k \tag{4}$$

for the LA mode along the y direction with the value of the square root giving the longitudinal speed of sound in the y direction. Finally, we get

$$\omega_{TA} = \sqrt{\frac{c_{66}}{\rho_{2D}}}k \tag{5}$$

for the in-plane TA modes in the x and y directions with the value of the square root giving the transverse speed of sound in those directions. In anisotropic plates, acoustic modes in an arbitrary in-plane direction have mixed LA and TA characters, and their speed varies in a complicated way with the direction [5].

As shown in the Appendix, the flexural ZA mode displays an unusual quadratic frequency dependence on the crystal momentum. Its frequency is given by

$$\omega_{ZA} = \sqrt{\frac{D}{\rho_{2D}}}k^2, \tag{6}$$

where the value of the flexural rigidity D depends on the bending direction in an anisotropic material.

The schematic dependence of the acoustic mode frequencies ω of a zero-thickness plate on the crystal momentum $\mathbf{k}$, given by Eqs. (3)–(6), is shown in Fig. 1(b). We note that these expressions, albeit not in the notation of the 2D elastic matrix, have been obtained previously [10–12].

Expressions describing the deformation of an elastic membrane can also be used to determine the frequency of the RBM. Previously derived theoretical expressions [13] and experimental observations are being used commonly as an indirect way to determine the diameter of carbon fullerenes and nanotubes [14].

As shown in the Appendix, we obtain

$$\omega_{C_n} = \frac{2}{d}\sqrt{\frac{2c_{11}}{\rho_{2D}}} \tag{7}$$

for the RBM frequency of a spherical C_n fullerene with diameter d. Similarly, the RBM frequency of a carbon nanotube (CNT) of radius d is given by

$$\omega_{\mathrm{CNT}} = \frac{2}{d}\sqrt{\frac{c_{11}}{\rho_{2D}}}. \tag{8}$$

IV. COMPUTATIONAL APPROACH TO DETERMINE THE ELASTIC CONSTANTS

We determine the elastic response of atomically thin graphene and phosphorene monolayers using *ab initio* DFT as implemented in the SIESTA [15] code. We used the Perdew-Burke-Ernzerhof [16] exchange-correlation functional, norm-conserving Troullier-Martins pseudopotentials [17], and a double-ζ basis including polarization orbitals. To determine the energy cost associated with in-plane distortions, we sampled the Brillouin zone of a 3D superlattice of noninteracting layers by a $20\times20\times1$ k-point grid [18]. To determine the strain energy associated with flexural motion, we constructed and optimized single-wall nanotubes and sampled their 3D superlattices by a $20\times1\times1$ k-point grid. We used a mesh cutoff energy of 180 Ry and an energy shift of 10 meV in our self-consistent total energy calculations, which has provided us with precision in the total energy of $\leqslant 2$ meV/atom.

V. RESULTS

A. Graphene

Graphene is known to display isotropic elastic behavior. Our DFT calculations yield the (3×3) 2D elastic stiffness matrix of Eq. (1),

$$\begin{pmatrix} c_{11} & c_{12} & 0 \\ c_{12} & c_{22} & 0 \\ 0 & 0 & c_{66} \end{pmatrix} = \begin{pmatrix} 352.6 & 59.6 & 0 \\ 59.6 & 352.6 & 0 \\ 0 & 0 & 146.5 \end{pmatrix} \text{N/m}. \quad (9)$$

These values are in very good agreement with experimental and other theoretical results [19], including the value of the Poisson ratio $\alpha = c_{12}/c_{11} = 0.17$, which is very close to the observed value of 0.19 based on high-resolution electron-energy-loss spectroscopy (HREELS) [20].

The calculated 2D mass density of graphene is $\rho_{2D} = 0.743 \times 10^{-6}$ kg/m^2 and the calculated value of the flexural rigidity $D = 1.40$ eV $= 0.224$ GPa nm^3 lies close to the previously estimated value [10] of $D \approx 1.0$ eV. Using the numerical values listed in Eq. (9) and the above value of D, we can determine the three acoustic branches of graphene near the Γ point using Eqs. (3)–(6). Our results are presented in Fig. 2(a), superposed on those of a more recent *ab initio* calculation [21] that agrees very well with the observed and fitted phonon spectra of graphene [22].

First of all, we notice excellent agreement with the linear LA and TA modes, which indicates that the calculated speed of sound agrees with the observation. Specifically, the calculated speed of sound with in-plane longitudinal polarization $v_{LA,th} = 22.1$ km/s agrees very well with the observed value of $v_{LA,\text{expt}} = 22.0$ km/s obtained using HREELS [20]. Similarly, the speed of sound with in-plane transverse polarization $v_{TA,th} = 14.2$ km/s agrees very well with the observed value [20] of $v_{TA,\text{expt}} = 14.0$ km/s.

Agreement between calculated and observed ZA modes indicates that the calculated flexural rigidity value correctly reproduces the elastic response of graphene to bending.

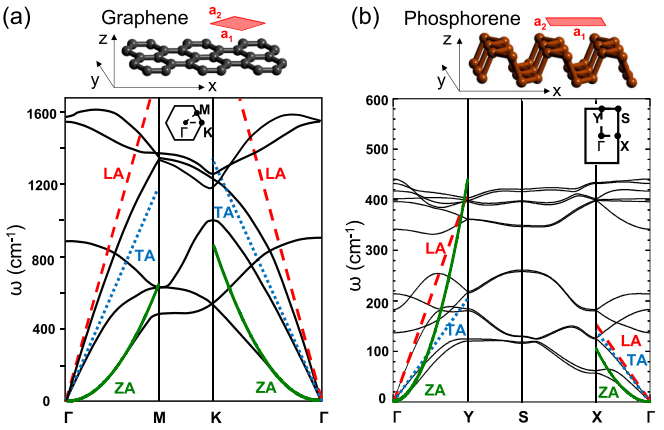

FIG. 2. Phonon spectra of (a) graphene, reproduced from Ref. [21] and (b) phosphorene, a monolayer of black phosphorus, reproduced from Ref. [23], shown by the solid lines. Superposed on the spectra are continuum results for the three acoustic phonon modes in different high-symmetry directions, evaluated near Γ, with the LA (dashed lines), in-plane TA (dotted lines), and the flexural acoustic ZA (solid lines) modes. Ball-and-stick models of the structure, including the primitive unit cells, are shown in the top panels. The Brillouin zones are shown as insets in the phonon spectra.

B. Phosphorene

Unlike graphene, phosphorene is strongly anisotropic. It is much softer under compression along the x (or $\mathbf{a}_1$) direction than along the y (or $\mathbf{a}_2$) direction. The optimized rectangular unit cell is defined by $a_1 = 4.63$ Å and $a_2 = 3.35$ Å according to our DFT studies. With four atoms per unit cell, the 2D mass density of phosphorene is $\rho_{2D} = 1.34 \times 10^{-6}$ kg/m^2. Our numerical values of $c_{11} = 24.4$ N/m and $c_{22} = 94.6$ N/m reflect the strong anisotropy in the in-plane longitudinal elastic response. The calculated speed of sound with LA polarization is $v_{LA_X,th} = 4.3$ km/s along the soft Γ-X direction and $v_{LA_Y,th} = 8.4$ km/s along the stiff Γ-Y direction.

The transverse acoustic phonon frequency depends on the in-plane shear and is described by our calculated value of $c_{66} = 22.1$ N/m. The corresponding speed of sound with TA polarization is $v_{TA,th} = 4.1$ km/s.

Finally, we find also the flexural rigidity to be highly anisotropic. We find $D(\Gamma\text{-}X) = 1.55$ eV $= 0.248$ GPa nm^3 when bending phosphorene along the x (or $\mathbf{a}_1$) direction, yielding a tube with its axis aligned along the y (or $\mathbf{a}_2$) direction. Bending along the y (or $\mathbf{a}_2$) direction, we find $D(\Gamma\text{-}Y) = 7.36$ eV $= 1.179$ GPa nm^3.

These data are sufficient to reproduce the three acoustic branches of phosphorene along the Γ-X and Γ-Y directions near Γ using Eqs. (3)–(6) and are presented in Fig. 2(b). In analogy to graphene, our results are superposed on phonon spectra, which—in the absence of experimental phonon spectra—are based on atomistic DFT calculations of phosphorene [23]. We notice particularly good agreement between the two approaches along the stiff Γ-Y direction. As we expand in the Discussion, the continuum results deviate from those of the atomistic study along the soft Γ-X direction, which—at

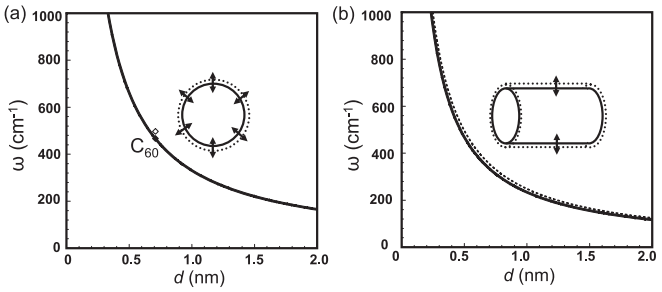

FIG. 3. RBM in (a) fullerenes and (b) carbon nanotubes as a function of their diameter d. Our prediction is shown by the solid line. Experimental and theoretical RBM frequencies for the only observed fullerene with spherical symmetry C_{60} are shown by the data points in (a). The experimentally well-established relationship [14,24] $\omega = 248\ \mathrm{cm}^{-1} \times (1\ \mathrm{nm}/d)$ in the nanotubes in (b) is represented by the dashed line, and our calculation is shown by the solid line.

close inspection—predicts small imaginary ZA frequencies near Γ.

C. Vibration spectra of carbon fullerenes and nanotubes

The RBM frequency ω_{RBM} of C_n fullerenes may be calculated using Eq. (7) and that of carbon nanotubes using Eq. (8) in combination with the elastic constants provided in the section on graphene. The expected dependence of ω_{RBM} on the diameter d is displayed in Fig. 3(a) for fullerenes and in Fig. 3(b) for CNTs. The RBM mode is Raman active, and its frequency is known to depend primarily on the diameter. Thus, the RBM frequency is commonly used to judge the diameter of carbon nanostructures.

According to Eq. (7), the RBM frequency of spherical fullerenes should scale inversely with their diameters. But only one spherical fullerene, namely, C_{60} with $d = 7.1$ Å forms a molecular solid. We find the predicted value of $\omega_{\mathrm{RBM},th}(C_{60}) = 467\ \mathrm{cm}^{-1}$ to lie very close to the observed RBM frequency of $\omega_{\mathrm{RBM,expt}}(C_{60}) = 497\ \mathrm{cm}^{-1}$.

The well-documented observed diameter dependence of the RBM in nanotubes [14] $\omega_{\mathrm{RBM,expt}}(\mathrm{CNT}) = 248\ \mathrm{cm}^{-1} \times (1\ \mathrm{nm}/d)$ is reproduced by the dashed line in Fig. 3(b). Based on continuum theory and Eq. (8), we find $\omega_{\mathrm{RBM},th}(\mathrm{CNT}) = 234\ \mathrm{cm}^{-1} \times (1\ \mathrm{nm}/d)$ in very good agreement with the observed behavior.

VI. DISCUSSION

So far, the most common description of a layer by continuum elasticity theory has been that of a finite-thickness plate consisting of a material characterized by a (6×6) elastic stiffness matrix. As we show here, this approach is unnecessarily cumbersome since every 2D system of finite thickness may be mapped onto an elastic membrane with the same mass density. The resistance of the realistic system, such as graphene or phosphorene, to stretching, shear, and bending becomes that of the elastic membrane. The advantage of this approach, which does not suffer from ambiguities about the "real" thickness of an atomic layer, has been discussed before [7,8]. The unconventional units of the 2D elastic stiffness matrix in Eq. (1) are well adapted to ultrathin layers.

Our approach appears particularly suitable when describing the ZA mode in soft atomically thin atomic layers, such as phosphorene. As mentioned earlier during the discussion of Fig. 2(b), the required precision of the dynamical matrix has not been reached in the calculation of phonon modes near Γ along the Γ-X direction [23]. This is a common shortcoming of *ab initio* phonon calculations in layered solids. Among the eigenvalues of the dynamical matrix, which are proportional to ω^2, the one associated with the ZA mode often turns out to be negative, yielding nominally an imaginary frequency, as a numerical artifact. The small error in the ZA frequency eigenvalue is also reflected in other close-lying eigenvalues, such as those of the LA and TA modes, at the same crystal momentum. This is clearly reflected in Fig. 2(b). We believe that the present continuum approach is much better adapted to describe long-wavelength acoustic modes and should be preferred to atomistic phonon calculations near Γ.

As seen in Fig. 2(b), the LA and TA mode frequencies are very similar along the soft Γ-X direction in phosphorene. This is unusual, but not unexpected in view of the accordionlike structure depicted in the ball-and-stick model in the top panel of Fig. 2(b). Making an analogy to a real accordion, it appears equally easy to produce a longitudinal and a transversal motion while the instrument is being played. Since the TA speed of sound is the same along the Γ-X and the Γ-Y directions, the TA mode is clearly distinguished in its softness from the LA mode along the hard Γ-Y direction. In this rigid direction in space, small imprecisions in the dynamical matrix play a much less important role than along the soft direction. Therefore, our continuum results agree well with the phonon frequencies obtained using the atomistic approach for all three acoustic branches.

In the Appendix section on the radial breathing motion of carbon nanostructures, we have shown in Eq. (A52) that the RBM frequency of nanotubes does not show a pure $1/d$ behavior as a function of the nanotube diameter. For single-wall carbon nanotubes with typical diameters between 1 nm and 2 nm, the value of the correction $4D/(c_{11}d^2)$ is indeed negligibly small in comparison to 1. This need not be the case in nanotubes of other substances with large values of D and small values of c_{11}. In postulated phosphorene nanotubes [25], c_{11} differs significantly from c_{22}, and D is strongly anisotropic.

Finally, we have shown in Eq. (2) how to estimate the value of D in a layered material by calculating the strain energy in nanotubes with a very large diameter d. Optimizing wide nanotubes using *ab initio* techniques is nontrivial. The values for D quoted in the section on phosphorene required DFT calculations containing more than 14 unit cells along the perimeter of phosphorene nanotubes bent along the soft x (or $\mathbf{a}_1$) direction. For nanotubes bent along the rigid y (or $\mathbf{a}_2$) direction, $D(d\to\infty)$ was extrapolated using 10, 12, 14, 16, and 18 unit cells along the perimeter of the corresponding phosphorene nanotubes.

VII. SUMMARY AND CONCLUSIONS

In conclusion, as a viable alternative to atomistic calculations of long-wavelength acoustic modes of atomically thin layers, which are known to converge very slowly, we have proposed a quantitatively predictive and physically intuitive

approach based on continuum elasticity theory. We describe a layer, independent of its thickness, by a membrane and characterize its elastic behavior by a (3×3) elastic matrix as well as the flexural rigidity D. We have derived simple quantitative expressions for frequencies of long-wavelength acoustic ZA and—for the sake of completeness—for the LA and TA modes. These frequencies are determined using 2D elastic constants obtained from *ab initio* DFT calculations for the deformation energy of unit cells with few atoms. We found that the calculated spectra accurately reproduce observed and calculated long-wavelength phonon spectra of graphene and phosphorene, the monolayer of black phosphorus. Our approach also correctly describes the observed dependence of the radial breathing mode frequency on the diameter of carbon fullerenes, such as C_{60} and carbon nanotubes.

ACKNOWLEDGMENTS

We acknowledge useful discussions with J. Guan and thank G. B. King for assistance with the artwork in Fig. 1. A.G.E. acknowledges financial support by the South African National Research Foundation. D.L. and D.T. acknowledge financial support from the NSF/AFOSR EFRI 2-DARE Grant No. EFMA-1433459.

APPENDIX

The most fundamental way to determine vibration motion in any system starts with a Lagrangian from which the Euler-Lagrange equations of motion can be derived by applying Hamilton's principle of least action. In the following, we determine the Lagrangians that describe stretching, shearing, and bending of an infinitely thin elastic plate. Using these Lagrange functions, we derive the equations of stretching, shearing, and bending motions of the plate. Finally, we derive the Lagrangian describing the radial breathing motions of carbon fullerenes and nanotubes and determine the corresponding equations of motion for the RBM in these nanostructures.

1. Lagrange function of an infinitely thin elastic plate under strain

a. Stretching

Let us consider a thin plate suspended on the xy plane and its response to in-plane tensile strain applied uniformly along the x direction,

$$\frac{du_x}{dx} = \text{const.} \tag{A1}$$

The resulting energy density caused by tensile strain along the x direction is then given by

$$U = \frac{1}{2} c_{11} \left(\frac{du_x}{dx} \right)^2, \tag{A2}$$

where c_{11} describes the elastic stiffness to tensile strain. In the harmonic regime, we will consider only small strain values. Releasing the strain will cause a vibration in the x direction with the velocity $v_x = du_x/dt$. Then, the kinetic-energy density will be given by

$$T = \frac{1}{2} \rho_{2D} \left(\frac{du_x}{dt} \right)^2, \tag{A3}$$

where ρ_{2D} is the 2D mass density. The Lagrangian density is then given by

$$\begin{aligned} \mathcal{L}\left(\frac{du_x}{dx}, \frac{du_x}{dt}, x, t \right) &= T - U \\ &= \frac{1}{2} \left[\rho_{2D} \left(\frac{du_x}{dt} \right)^2 - c_{11} \left(\frac{du_x}{dx} \right)^2 \right]. \end{aligned} \tag{A4}$$

In an anisotropic plate, the x and y directions are not equivalent. To describe the y response to in-plane tensile strain applied uniformly along the y direction, we have to replace x by y and c_{11} by c_{22} in Eqs. (A1)–(A4), yielding the Lagrangian density,

$$\begin{aligned} \mathcal{L}\left(\frac{du_y}{dy}, \frac{du_y}{dt}, y, t \right) &= T - U \\ &= \frac{1}{2} \left[\rho_{2D} \left(\frac{du_y}{dt} \right)^2 - c_{22} \left(\frac{du_y}{dy} \right)^2 \right]. \end{aligned} \tag{A5}$$

b. Shearing

The derivation of the Euler-Lagrange equation for the shear motion is very similar to that for the stretching motion. The main difference is that the displacement u is normal to the propagation direction. To obtain the corresponding equations, we need to replace u_x by u_y and c_{11} by c_{66} in Eqs. (A1)–(A4). The Lagrangian density is then given by

$$\begin{aligned} \mathcal{L}\left(\frac{du_y}{dx}, \frac{du_y}{dt}, x, t \right) &= T - U \\ &= \frac{1}{2} \left[\rho_{2D} \left(\frac{du_y}{dt} \right)^2 - c_{66} \left(\frac{du_y}{dx} \right)^2 \right]. \end{aligned} \tag{A6}$$

c. Bending

Bending a thin plate suspended on the xy plane in order to achieve a radius of curvature R requires displacements $u_z(x)$ along the normal z direction that are described by

$$\frac{d^2 u_z}{dx^2} = \frac{1}{R}. \tag{A7}$$

The resulting bending energy density is then given by

$$U = \frac{1}{2} D \left(\frac{d^2 u_z}{dx^2} \right)^2, \tag{A8}$$

where D is the flexural rigidity. In the harmonic regime, we will consider only small strain values corresponding to $R \to \infty$. Releasing the strain will cause a vibration in the z direction with the velocity $v_z = du_z/dt$. Then, the

kinetic-energy density will be given by

$$T = \frac{1}{2}\rho_{2D}\left(\frac{du_z}{dt}\right)^2, \tag{A9}$$

where ρ_{2D} is the 2D mass density. This leads to the Lagrangian density,

$$\mathcal{L}\left(\frac{d^2u_z}{dx^2},\frac{du_z}{dt},x,t\right) = T - U = \frac{1}{2}\left[\rho_{2D}\left(\frac{du_z}{dt}\right)^2 - D\left(\frac{d^2u_z}{dx^2}\right)^2\right]. \tag{A10}$$

2. Derivation of Euler-Lagrange equations of motion for deformations of an infinitely thin elastic plate using Hamilton's principle

a. Stretching

The Lagrangian specified in Eq. (A4) has the form $\mathcal{L}(du_x/dx,du_x/dt,x,t)$. In this case, we have two independent variables x and t and can define the action S by

$$S = \int_{t_1}^{t_2} dt \int_{x_1}^{x_2} dx\, \mathcal{L}\left(\frac{du_x}{dx},\frac{du_x}{dt},x,t\right). \tag{A11}$$

Hamilton's principle of least action yields

$$\delta S = \delta \int_{t_1}^{t_2} dt \int_{x_1}^{x_2} dx\, \mathcal{L}\left(\frac{du_x}{dx},\frac{du_x}{dt},x,t\right) = 0. \tag{A12}$$

This can be modified to

$$\delta S = \int_{t_1}^{t_2} dt \int_{x_1}^{x_2} dx \left[\mathcal{L}\left(\frac{du_x}{dx}+\delta\frac{du_x}{dx},\frac{du_x}{dt}+\delta\frac{du_x}{dt},x,t\right) - \mathcal{L}\left(\frac{du_x}{dx},\frac{du_x}{dt},x,t\right)\right]. \tag{A13}$$

and

$$\delta S = \int_{t_1}^{t_2} dt \int_{x_1}^{x_2} dx \left[\frac{\partial\mathcal{L}}{\partial\frac{du_x}{dx}}\delta\frac{du_x}{dx} + \frac{\partial\mathcal{L}}{\partial\frac{du_x}{dt}}\delta\frac{du_x}{dt}\right]. \tag{A14}$$

This expression can be reformulated to

$$\delta S = \int_{t_1}^{t_2} dt \int_{x_1}^{x_2} dx \left[\frac{d}{dt}\left(\frac{\partial\mathcal{L}}{\partial\frac{du_x}{dt}}\right) + \frac{d}{dx}\left(\frac{\partial\mathcal{L}}{\partial\frac{du_x}{dx}}\right)\right]\delta u_x. \tag{A15}$$

For δS to vanish, the quantity in the square brackets in Eq. (A15) must vanish. This leads to the Euler-Lagrange equation,

$$\frac{d}{dt}\left(\frac{\partial\mathcal{L}}{\partial\frac{du_x}{dt}}\right) + \frac{d}{dx}\left(\frac{\partial\mathcal{L}}{\partial\frac{du_x}{dx}}\right) = 0. \tag{A16}$$

Inserting the Lagrangian of Eq. (A4) in the Euler-Lagrange Eq. (A16) yields the wave equation for longitudinal in-plane vibrations,

$$\rho_{2D}\frac{d^2u_x}{dt^2} - c_{11}\frac{d^2u_x}{dx^2} = 0. \tag{A17}$$

This wave equation can be solved using the ansatz,

$$u_x = u_{x,0}e^{i(kx-\omega t)} \tag{A18}$$

to yield

$$\rho_{2D}\omega^2 = c_{11}k^2. \tag{A19}$$

This finally translates to the desired form

$$\omega = \sqrt{\frac{c_{11}}{\rho_{2D}}}k, \tag{A20}$$

which is identical to Eq. (3).

In an anisotropic plate, we need to use the Lagrangian of Eq. (A5) to describe motion along the y direction and obtain

$$\omega = \sqrt{\frac{c_{22}}{\rho_{2D}}}k, \tag{A21}$$

which is identical to Eq. (4).

b. Shearing

The Lagrangian $\mathcal{L}(du_y/dx,du_y/dt,x,t)$ in Eq. (A6), which describes the shearing motion, has the same form as the Lagrangian in Eq. (A4). To obtain the equations for shear motion from those for stretching motion, we need to replace u_x by u_y and c_{11} by c_{66} in Eqs. (A11)–(A20). Thus, the equation for shear motion becomes

$$\omega = \sqrt{\frac{c_{66}}{\rho_{2D}}}k, \tag{A22}$$

which is identical to Eq. (5).

c. Bending

The Lagrangian specified in Eq. (A10) has the unconventional form $\mathcal{L}(d^2u_z/dx^2,du_z/dt,x,t)$. In this case, we have two independent variables, namely, x and t and can define the action S by

$$S = \int_{t_1}^{t_2} dt \int_{x_1}^{x_2} dx\, \mathcal{L}\left(\frac{d^2u_z}{dx^2},\frac{du_z}{dt},x,t\right). \tag{A23}$$

Hamilton's principle of least action yields

$$\delta S = \delta \int_{t_1}^{t_2} dt \int_{x_1}^{x_2} dx\, \mathcal{L}\left(\frac{d^2u_z}{dx^2},\frac{du_z}{dt},x,t\right) = 0. \tag{A24}$$

This can be modified to

$$\delta S = \int_{t_1}^{t_2} dt \int_{x_1}^{x_2} dx \left[\mathcal{L}\left(\frac{d^2u_z}{dx^2}+\delta\frac{d^2u_z}{dx^2},\frac{du_z}{dt}+\delta\frac{du_z}{dt},x,t\right) - \mathcal{L}\left(\frac{d^2u_z}{dx^2},\frac{du_z}{dt},x,t\right)\right], \tag{A25}$$

and

$$\delta S = \int_{t_1}^{t_2} dt \int_{x_1}^{x_2} dx \left[\frac{\partial\mathcal{L}}{\partial\frac{d^2u_z}{dx^2}}\delta\frac{d^2u_z}{dx^2} + \frac{\partial\mathcal{L}}{\partial\frac{du_z}{dt}}\delta\frac{du_z}{dt}\right]. \tag{A26}$$

Finally, we can rewrite this expression as

$$\delta S = \int_{t_1}^{t_2} dt \int_{x_1}^{x_2} dx \left[\frac{d}{dt}\left(\frac{\partial\mathcal{L}}{\partial\frac{du_z}{dt}}\right) - \frac{d^2}{dx^2}\left(\frac{\partial\mathcal{L}}{\partial\frac{d^2u_z}{dx^2}}\right)\right]\delta u_z. \tag{A27}$$

For δS to vanish, the quantity in the square brackets in Eq. (A27) must vanish. This leads to the Euler-Lagrange

equation,

$$\frac{d}{dt}\left(\frac{\partial\mathcal{L}}{\partial\frac{du_z}{dt}}\right)-\frac{d^2}{dx^2}\left(\frac{\partial\mathcal{L}}{\partial\frac{d^2u_z}{dx^2}}\right)=0. \tag{A28}$$

Inserting the Lagrangian of Eq. (A10) for flexural motion in the Euler-Lagrange Eq. (A28) yields the wave equation for flexural vibrations,

$$\rho_{2D}\frac{d^2u_z}{dt^2}+D\frac{d^4u_z}{dx^4}=0. \tag{A29}$$

This wave equation can be solved using the ansatz,

$$u_z=u_{z,0}e^{i(kx-\omega t)} \tag{A30}$$

to yield

$$\rho_{2D}\omega^2=Dk^4. \tag{A31}$$

This finally translates to the desired form

$$\omega=\sqrt{\frac{D}{\rho_{2D}}}k^2, \tag{A32}$$

which is identical to Eq. (6).

3. Radial breathing mode of spherical fullerenes

Let us consider a spherical fullerene molecule, such as C_{20} or C_{60}, with the equilibrium radius R. Except for the presence of 12 pentagons, the surface is covered by hexagonal carbon rings so that the 2D mass density ρ_{2D} can be taken as that of graphene. Similarly, R can be estimated using the number of C atoms in the fullerene and the unit-cell area in graphene. According to continuum elasticity theory, the total bending strain energy of any such spherical fullerene, independent of R, is given by [26]

$$U_b=4\pi D(1+\alpha), \tag{A33}$$

where D is the flexural rigidity and α is the Poisson ratio of graphene. In other words, changing the radius of the fullerene by δR will not affect the total bending energy.

Allowing the equilibrium radius R of the fullerene to change by δR results, on the other hand, in a quadratic increase in the tensile strain energy,

$$U_t=2\times\frac{1}{2}[4\pi R^2c_{11}]\left(\frac{\delta R}{R}\right)^2. \tag{A34}$$

The (radial) kinetic energy of a radially expanding or contracting fullerene, shown schematically in the inset of Fig. 3(a), is given by

$$T=\frac{1}{2}[4\pi R^2\rho_{2D}]\left(\frac{d}{dt}\delta R\right)^2, \tag{A35}$$

and the Lagrangian by

$$\begin{aligned}\mathcal{L}&=T-U\\&=T-U_t\\&=\frac{1}{2}[4\pi R^2\rho_{2D}]\left(\frac{d}{dt}\delta R\right)^2-[4\pi R^2c_{11}]\left(\frac{\delta R}{R}\right)^2\\&=4\pi R^2\left[\frac{1}{2}\rho_{2D}\left(\frac{d}{dt}\delta R\right)^2-c_{11}\left(\frac{\delta R}{R}\right)^2\right].\end{aligned} \tag{A36}$$

Hamilton's principle of least action,

$$\frac{\partial\mathcal{L}}{\partial(\delta R)}-\frac{d}{dt}\left(\frac{\partial\mathcal{L}}{\partial\left(\frac{d}{dt}\delta R\right)}\right)=0 \tag{A37}$$

leads with the Lagangian of Eq. (A36) to the Euler-Lagrange equation,

$$-c_{11}\frac{2\delta R}{R^2}=\rho_{2D}\frac{d^2}{dt^2}\delta R. \tag{A38}$$

With the ansatz,

$$\delta R=\delta R_0e^{i\omega t}, \tag{A39}$$

we obtain

$$\omega=\frac{1}{R}\sqrt{\frac{2c_{11}}{\rho_{2D}}}, \tag{A40}$$

which is identical to Eq. (7).

4. Radial breathing mode of carbon nanotubes

Let us now consider a carbon nanotube that has been rolled up from a rectangular graphene nanoribbon of width $2\pi R_0$, length L, and the 2D mass density ρ_{2D}. According to continuum elasticity theory, the total bending strain energy of any such nanotube is given by [26]

$$U_b=\frac{\pi DL}{R_0}, \tag{A41}$$

where D is the flexural rigidity of graphene. Increasing the radius by the small amount δR, whereas still $\delta R/R_0\ll 1$, changes the potential energy of the nanotube with respect to the value at R_0 by

$$\Delta U_b(\delta R)=\frac{\pi DL}{R_0}\left[-\frac{\delta R}{R_0}+\left(\frac{\delta R}{R_0}\right)^2\right], \tag{A42}$$

where higher than quadratic terms have been neglected in the Taylor expansion.

We consider the initial nanotube of radius R_0 to be free of tensile strain energy. In this case, the change in tensile strain energy associated with the radius increase by δR is

$$\Delta U_t(\delta R)=\frac{1}{2}[2\pi R_0c_{11}]L\left(\frac{\delta R}{R_0}\right)^2. \tag{A43}$$

The equilibrium value of δR can be obtained by minimizing $\Delta U_b+\Delta U_t$,

$$\frac{\partial(\Delta U_b+\Delta U_t)}{\partial(\delta R)}=0. \tag{A44}$$

This leads to

$$\delta R\approx\frac{D}{2c_{11}R_0}, \tag{A45}$$

and the equilibrium value of the nanotube radius becomes $R=R_0+\delta R$,

$$R=R_0\left(1+\frac{D}{2c_{11}R_0^2}\right). \tag{A46}$$

R is the radius, around which the RBM vibrations take place. We use the total potential energy U of the nanotube at the

equilibrium radius R as the reference energy. Then, changing the equilibrium nanotube radius R by an arbitrarily small value of δR increases the potential energy of the nanotube by

$$U = \frac{1}{2}[2\pi RL]\left(\frac{D}{R^4} + \frac{c_{11}}{R^2}\right)(\delta R)^2. \tag{A47}$$

The (radial) kinetic energy of a radially expanding or contracting nanotube, shown schematically in the inset of Fig. 3(b), is given by

$$T = \frac{1}{2}[2\pi R\rho_{2D}L]\left(\frac{d}{dt}\delta R\right)^2. \tag{A48}$$

The Lagrangian for this motion is

$$\begin{aligned}\mathcal{L} &= T - U \\ &= [\pi R\rho_{2D}L]\left(\frac{d}{dt}\delta R\right)^2 - [\pi RL]\left(\frac{D}{R^4} + \frac{c_{11}}{R^2}\right)(\delta R)^2.\end{aligned} \tag{A49}$$

Using Hamilton's principle of Eq. (A37), we get the Euler-Lagrange equation,

$$\rho_{2D}\frac{d^2(\delta R)}{dt^2} = -\left(\frac{D}{R^4} + \frac{c_{11}}{R^2}\right)\delta R. \tag{A50}$$

Using the ansatz,

$$\delta R = \delta R_0 e^{i\omega t}, \tag{A51}$$

and referring to the nanotube diameter $d = 2R$, we obtain

$$\omega = \frac{2}{d}\sqrt{\frac{c_{11}}{\rho_{2D}}\left(1 + \frac{D}{c_{11}R^2}\right)}. \tag{A52}$$

For a nanotube with a typical diameter of $d = 1$ nm, using the values of c_{11} and D for graphene, we find that the bending correction $4D/(c_{11}d^2) \approx 1 \times 10^{-3}$ is negligibly small. In this case, we obtain

$$\omega = \frac{2}{d}\sqrt{\frac{c_{11}}{\rho_{2D}}}, \tag{A53}$$

which is identical to Eq. (8).

[1] B. Peng, H. Zhang, H. Shao, Y. Xu, R. Zhang, and H. Zhu, The electronic, optical, and thermodynamic properties of borophene from first-principles calculations, J. Mater. Chem. C **4**, 3592 (2016).

[2] W. Yu, C.-Y. Niu, Z. Zhu, X. Wang, and W.-B. Zhang, Atomically thin binary V-V compound semiconductor: A first-principles study, J. Mater. Chem. C **4**, 6581 (2016).

[3] A. K. Majee and Z. Aksamija, Length divergence of the lattice thermal conductivity in suspended graphene nanoribbons, Phys. Rev. B **93**, 235423 (2016).

[4] A. E. H. Love, *A Treatise on the Mathematical Theory of Elasticity* (Cambridge University Press, Cambridge, U.K., 1927).

[5] A. A. Maznev and A. G. Every, Focusing of acoustic modes in thin anisotropic plates, Acta Acustica **3**, 387 (1995).

[6] P. Malekzadeh, M. R. Golbahar Haghighi, and M. Shojaee, Nonlinear free vibration of skew nanoplates with surface and small scale effects, Thin-Walled Struct. **78**, 48 (2014).

[7] Q. Lu and R. Huang, Nonlinear mechanics of single-atomic-layer graphene sheets, Int. J. Appl. Mech. **1**, 443 (2009).

[8] P. Lambin, Elastic properties and stability of physisorbed graphene, Appl. Sci. **4**, 282 (2014).

[9] B. Arash and Q. Wang, A review on the application of nonlocal elastic models in modeling of carbon nanotubes and graphenes, in *Modeling of Carbon Nanotubes, Graphene and Their Composites*, edited by I. Konstantinos Tserpes and N. Silvestre (Springer International, Cham, 2014), p. 57.

[10] A. H. Castro Neto, F. Guinea, N. M. R. Peres, K. S. Novoselov, and A. K. Geim, The electronic properties of graphene, Rev. Mod. Phys. **81**, 109 (2009).

[11] P. M. Chaikin and T. C. Lubensky, *Principles of Condensed Matter Physics* (Cambridge University Press, Cambridge, U.K., 1995).

[12] D. Nelson, T. Piran, and S. Weinberg, *Statistical Mechanics of Membranes and Surfaces*, 2nd ed. (World Scientific, Singapore, 2004), p. 262.

[13] H. Suzuura and T. Ando, Phonons and electron-phonon scattering in carbon nanotubes, Phys. Rev. B **65**, 235412 (2002).

[14] D. Tománek, *Guide Through the Nanocarbon Jungle* (IOP, Bristol, U.K., 2014).

[15] E. Artacho, E. Anglada, O. Dieguez, J. D. Gale, A. Garcia, J. Junquera, R. M. Martin, P. Ordejon, J. M. Pruneda, D. Sanchez-Portal, and J. M. Soler, The siesta method; developments and applicability, J. Phys.: Condens. Matter **20**, 064208 (2008).

[16] J. P. Perdew, K. Burke, and M. Ernzerhof, Generalized Gradient Approximation Made Simple, Phys. Rev. Lett. **77**, 3865 (1996).

[17] N. Troullier and J. L. Martins, Efficient pseudopotentials for plane-wave calculations, Phys. Rev. B **43**, 1993 (1991).

[18] H. J. Monkhorst and J. D. Pack, Special points for brillouin-zone integrations, Phys. Rev. B **13**, 5188 (1976).

[19] K. V. Zakharchenko, M. I. Katsnelson, and A. Fasolino, Finite Temperature Lattice Properties of Graphene Beyond the Quasiharmonic Approximation, Phys. Rev. Lett. **102**, 046808 (2009).

[20] A. Politano, A. Raimondo Marino, D. Campi, D. Farías, R. Miranda, and G. Chiarello, Elastic properties of a macroscopic graphene sample from phonon dispersion measurements, Carbon **50**, 4903 (2012).

[21] L. Wirtz and A. Rubio, The phonon dispersion of graphite revisited, Solid State Commun. **131**, 141 (2004).

[22] R. A. Jishi, L. Venkataraman, M. S. Dresselhaus, and G. Dresselhaus, Phonon modes in carbon nanotubules, Chem. Phys. Lett. **209**, 77 (1993).

[23] Z. Zhu and D. Tománek, Semiconducting Layered Blue Phosphorus: A Computational Study, Phys. Rev. Lett. **112**, 176802 (2014).

[24] A. M. Rao, E. Richter, S. Bandow, B. Chase, P. C. Eklund, K. A. Williams, S. Fang, K. R. Subbaswamy, M. Menon, A. Thess, R. E. Smalley, G. Dresselhaus, and M. S. Dresselhaus, Diameter-selective Raman scattering from vibrational modes in carbon nanotubes, Science **275**, 187 (1997).

[25] J. Guan, Z. Zhu, and D. Tománek, High Stability of Faceted Nanotubes and Fullerenes of Multiphase Layered Phosphorus: A Computational Study, Phys. Rev. Lett. **113**, 226801 (2014).

[26] D. Tomanek, W. Zhong, and E. Krastev, Stability of multishell fullerenes, Phys. Rev. B **48**, 15461 (1993).